PNAS RESEARCH ARTICLE BIOCHEMISTRY
BIOPHYSICS AND COMPUTATIONAL BIOLOGY

Spatially regulated mRNA translation enables functional membrane protein integration in synthetic cells

Hang Fu[a,b,1], Lijuan Ma[a,b,1], Chunhua Xu[a], Jinghua Li[a], Haochen Ouyang[a,c], Congbao Xie[a], Yunhai Sun[a,c], Yuanxiao Tao[a,c], Hao Wang[a,c], Shuxin Hu[a], Meifang Fu[c,d], Hai Zheng[c,d], Honghong Zhang[c,d], Chenli Liu[c,d], Fangfu Ye[a,b,c], Yan Qiao[c,e], Ming Li[a,c,2], and Ying Lu[a,c,2]

Affiliations are included on p. 9.

Edited by James Hurley, University of California Berkeley, Berkeley, CA; received July 2, 2025; accepted December 20, 2025

Synthetic cells aim to emulate living systems by reconstituting essential cellular processes within lipid-bound architectures. However, their functional complexity remains constrained by a key challenge: the synthesis and correct integration of hydrophobic membrane proteins via cell-free approaches. Here, inspired by natural cells, we developed a spatially regulated translation strategy in which membrane-anchored mRNAs recruit ribosomes to drive the cotranslational insertion of membrane proteins into lipid bilayers. This design enables efficient in situ synthesis and integration of multiple transmembrane proteins within giant unilamellar vesicles, supporting selective small-molecule transport across membranes. Importantly, the method allows for precise stoichiometric control of membrane protein composition. Together, this work establishes a minimal yet versatile framework for the direct synthesis and integration of membrane proteins, advancing the construction of functional synthetic cells.

synthetic cells | membrane proteins | cell-free protein synthesis

Significance

A major challenge in synthetic cell construction is the de novo synthesis and incorporation of membrane proteins into the lipid bilayer. In this study, we introduce a concept of membrane-proximal spatial constraint on messenger RNA (mRNA) translation to direct protein insertion into lipid bilayers. By recapitulating the spatial control mechanism, our system enables programmable and efficient expression of membrane proteins in a functional state. This strategy provides a previously unexplored route for building synthetic cells with membrane-based functions, offering a conceptual and technical advance in bottom–up synthetic biology.

Synthetic cells represent a crucial frontier in synthetic biology, striving to encapsulate life-like functionalities within engineered lipid compartments (1–3). By employing a bottom–up molecular approach to construct and regulate integrated genetic elements, researchers have enhanced their ability to design and control synthetic cells. A central challenge in this endeavor is the reconstitution of membrane proteins—dynamic molecular machines responsible for selective transport, signal transduction, and structural integrity (4–8). These characteristics position synthetic cells as a modular and adaptable platform with potential applications in medicine, biosensing, biomanufacturing, and related fields.

Current strategies for membrane protein integration primarily rely on in vitro reconstitution methods, such as detergent-mediated solubilization and nanoliposome fusion, which facilitate the incorporation of purified proteins into lipid vesicles (9–14). Despite significant advances, these approaches still face critical limitations. During detergent-mediated solubilization and membrane integration, proteins often suffer from denaturation, misfolding, or incorrect insertion, resulting in compromised or lost functionality. In addition, the efficiency of incorporation varies widely depending on the specific combinations of membrane proteins and detergents, making it difficult to quantitatively control the protein stoichiometry within the membrane. Residual detergents or organic solvents may further impair the structural integrity and long-term stability of the lipid bilayer. More fundamentally, these approaches rely on the external, static insertion of prepurified proteins, lacking the capacity for dynamic, on-demand synthesis and regulation of membrane proteins within synthetic cells. This constraint severely limits the development of synthetic cellular systems capable of life-like behaviors such as environmental sensing, adaptive response, and autonomous regulation.

While commercially available cell-free protein expression (CFPE) systems demonstrated remarkable efficacy in producing diverse soluble proteins (15–17), the in situ synthesis and functional integration of hydrophobic membrane proteins within synthetic cells remain a critical unresolved challenge. Unlike cytosolic proteins, hydrophobic interactions make membrane proteins highly susceptible to misfolding and aggregation when exposed to aqueous environments (Fig. 1*A*). In natural cells, the translation process is tightly coupled with the membrane insertion to prevent hydrophobic collapse via the Sec–signal recognition particle (SRP) pathway or YidC (Fig. 1*A*) (18–23). Reconstituting the SRP-mediated targeting within micrometer-scale vesicles requires precise spatial coordination and stoichiometric balance among the multiple components, making it highly complex. Alternative strategies have achieved partial success by bypassing the native mechanisms. For instance, confining the protein synthesis to submicron vesicles (<1 μm) statistically enhances the proximity between ribosomes and membranes, facilitating the passive insertion of small transmembrane domains (24).

Author contributions: H.F., M.L., and Y.L. designed research; H.F., L.M., C. Xu, H.O., C. Xie, F.Y., and Y.Q. performed research; H.F., J.L., H.W., S.H., M.F., H. Zheng, H. Zhang, and C.L. contributed new reagents/analytic tools; H.F., Y.S., Y.T., and M.F. analyzed data; and H.F., Y.Q., M.L., and Y.L. wrote the paper.

The authors declare no competing interest.

This article is a PNAS Direct Submission.

Copyright © 2026 the Author(s). Published by PNAS. This article is distributed under Creative Commons Attribution-NonCommercial-NoDerivatives License 4.0 (CC BY-NC-ND).

[1]H.F. and L.M. contributed equally to this work.

[2]To whom correspondence may be addressed. Email: mingli@iphy.ac.cn or yinglu@iphy.ac.cn.

This article contains supporting information online at https://www.pnas.org/lookup/suppl/doi:10.1073/pnas.2517323123/-/DCSupplemental.

Published January 21, 2026.

Downloaded from https://www.pnas.org by CAS CONSORTIUM CHINESE ACADEMY OF SCIENCES on January 21, 2026 from IP address 159.226.35.236.

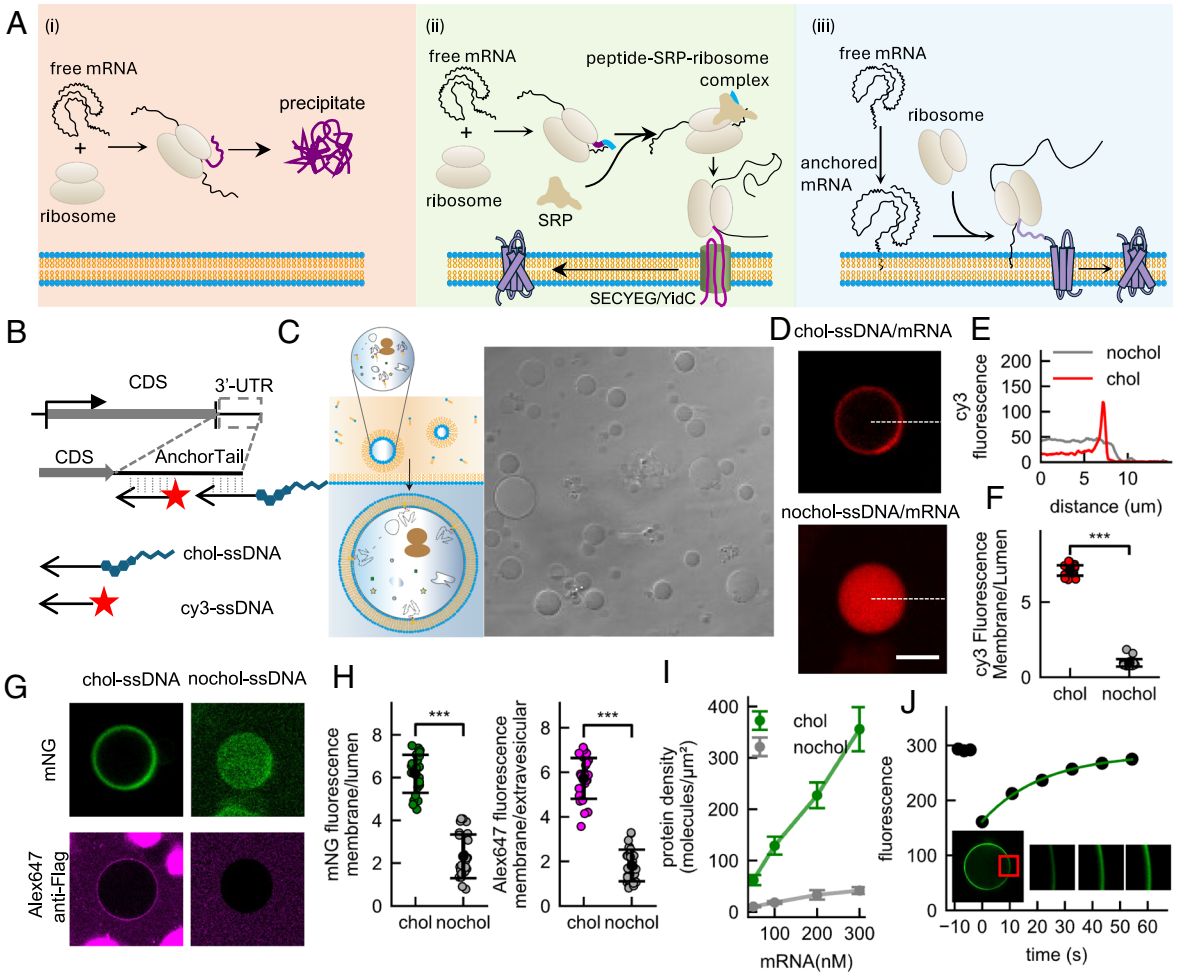

Fig. 1. Spatial regulation of membrane protein translation in GUVs. (*A*) Schematic illustration of three modes of membrane protein synthesis from mRNA: (*i*) in aqueous solution, hydrophobic membrane proteins misfold and aggregate posttranslation; (*ii*) in cells, membrane protein translation and insertion are co-translationally mediated by the SRP pathway; (*iii*) membrane-proximal translation of mRNA strategy proposed in this study. (*B*) Design of membrane-targeted mRNA complexes. (*C*) Schematic of cell-sized GUV synthesis. (*D*) Representative fluorescence images of GUVs containing cholesterol-modified (*Top*) or unmodified (*Bottom*) nucleic acid complexes. (*E*) Radial fluorescence intensity profiles quantifying membrane localization efficiency. (*F*) Quantification of membrane-to-lumen fluorescence intensity ratios for 25 GUVs per condition (mean ± quartiles). (*G*) Representative image of a GUV showing membrane-localized mNG-labeled Fo subunit a (green) and membrane-associated Alexa Fluor® 647 anti-Flag antibody (red). (*H*) Quantification of membrane-to-lumen (*Left*) and membrane-to-solution (*Right*) fluorescence intensity ratios derived from radial fluorescence profiles of individual GUVs. Green fluorescence (*Left*) corresponds to mNG-labeled Fo subunit a, indicating membrane localization. Red fluorescence (*Right*) corresponds to Alexa Fluor® 647 anti-Flag staining, reflecting the membrane accessibility of the tagged protein. Data represent 25 GUVs per condition. Box plots show the mean (open square), median, and quartiles. (*I*) Increasing the concentration of encapsulated mRNA complexes led to a proportional increase in the density of membrane-localized proteins Data represent more than 20 GUVs per condition. (*J*) Diffusion of synthetic membrane proteins in GUV membranes assessed by FRAP. Representative images show the prebleach, bleached (red box), and recovery regions. The plot shows normalized fluorescence recovery (black squares) and fitted curve (green). (Scale bar, 10 μm.)

However, the small reaction volumes magnify stochastic fluctuations in the initial component concentrations, destabilizing the metabolic networks during extended expression. Researchers have also employed membrane-anchored engineered ribosomes to tether translation machinery to lipid surfaces, but they are often incompatible with commercial CFPE systems and may perturb the ribosome conformational dynamics (25). Even in the absence of dedicated insertion machineries such as SecYEG or YidC, recent studies have shown that α-helical membrane proteins can spontaneously integrate into lipid bilayers when the translation occurs in close spatial proximity to the membrane (26, 27). This process follows a kinetic "capture" mechanism, whereby the nascent hydrophobic segments rapidly partition into the bilayer upon emergence from the ribosome, preventing aggregation or misfolding in the aqueous phase. The efficiency of this spontaneous cotranslational insertion depends largely on the frequency and duration of the ribosome–membrane encounters (27–30). These insights suggest that enhancing the local coupling between the translation and the membrane could markedly increase the success rate of membrane integration. These challenges underscore the need for a versatile, sequence-independent platform that couples translation with membrane integration. RNA-based regulatory elements offer unique advantages in this context, as they are directly transcribed, genetically encodable, and readily programmable. In natural cells, mRNAs exhibit distinct subcellular spatial distributions (31), enabling precise spatiotemporal control of gene expression (32–40). Inspired by the observation that some membrane-protein-encoding mRNAs localize near membranes independent of ribosomes, we hypothesized that membrane-anchored mRNAs could recruit ribosomes to form nanoscale translation zones, where nascent peptides immediately interact with the lipid bilayer. Leveraging the physicochemical affinity of hydrophobic residues for lipid environments (41–44), such cotranslational insertion could enable efficient membrane integration.

In this study, we developed an mRNA-based spatial translation platform that enables robust synthesis and integration of diverse α-helical membrane proteins within giant unilamellar vesicles

Downloaded from https://www.pnas.org by CAS CONSORTIUM CHINESE ACADEMY OF SCIENCES on January 21, 2026 from IP address 159.226.35.236.

(GUVs). Specifically, we designed a 3′ untranslated region (3′UTR)-encoded mRNA localization system that utilizes chemically modified nucleic acids and sequence-specific hybridization to direct translation toward the membrane, allowing efficient protein synthesis and integration in synthetic cells. Extending this system, we further synthesized functional transmembrane transporters to enable selective uptake of defined substrates. By modulating the relative abundance of membrane-targeted mRNAs encoding different proteins, we decoupled template dosage from protein stoichiometry within membranes, enabling fine-tuned control over membrane composition. Overall, our approach enhances membrane protein expression and integration without requiring modifications to protein sequences or ribosomal components, ensuring full compatibility with existing CFPE toolkits.

Results

Enhancing Membrane Protein Integration via Membrane-Proximal Translation. To address the concept described above (Fig. 1*A*), we developed a cholesterol-conjugated single-stranded DNA (chol-ssDNA) hybridization strategy. We engineered a 60-nucleotide sequence, termed "AnchorTail," into the 3'UTR of the target mRNA. This sequence included two functional domains: 1) a 20-nucleotide cholesterol binding domain complementary to chol-ssDNA, and 2) a 20-nucleotide visualization domain for conjugation with Cy3-conjugated ssDNA (Cy3-ssDNA) (Fig. 1*B*). Following in vitro transcription, which yielded >90% pure AnchorTail-mRNA, we produced a triple-hybrid complex through gradient annealing at a 1:1:1 molar ratio (mRNA: chol-ssDNA: Cy3-ssDNA). Distinct membrane binding properties were confirmed at the single-molecule level by the total internal reflection fluorescence (TIRF) microscopy (*SI Appendix*, Fig. S1). Quantitative analysis showed a significant increase in point density for chol-ssDNA complexes (0.15 counts/μm^2) compared to controls (~0 counts/μm^2) at a 100 pM triple-hybrid complex, confirming cholesterol-dependent membrane anchor. Subsequent encapsulation of the annealed complex (200 nM) within GUVs via inverse emulsion enabled spatial distribution analysis through confocal microscopy (Fig. 1*C*). The ratio between the fluorescence in the vesicular lumen and that at the membrane (*SI Appendix*, Fig. S2) indicated a 11-fold increase in membrane localization of the mRNAs with cholesterol modification (10.4 ± 1.1 vs. 1.0 ± 0.2) (Fig. 1 *D–F*). Selective nuclease digestion further confirmed that more than 80% of the complexes were bound to the inner membrane surface (*SI Appendix*, Fig. S3). These results conclusively demonstrate that the cholesterol mediated hybridization at the 3'UTR enables precise spatial regulation of mRNA distribution, achieving predominant localization near the phospholipid membrane in the synthetic cellular systems.

Building on the validated mRNA anchoring strategy, we designed a chimeric mRNA encoding a FLAG-tagged ATP synthase Fo subunit a, fused with mNeonGreen (mNG) and AnchorTail (FLAG-atpB-mNG-AnchorTail). After in vitro transcription and purification, we coencapsulated 50 to 300 nM triple-hybrid complex together with a PURE cell-free translation system into GUVs via inverse emulsion (Fig. 1*F*). Following a 3-h incubation at 37 °C, membrane protein synthesis occurred. The confocal imaging revealed a distinct spatial distribution of the synthesized proteins (Fig. 1*G*). As the concentration of the encapsulated complex increased, the amount of the membrane-associated protein also rose proportionally, demonstrating that the expression level can be predictably tuned through the density of the membrane binding mRNAs. The immunostaining with the Alexa Fluor® 647 conjugated anti-FLAG antibodies confirmed the correct transmembrane topology. The colocalization of the mNGs and the antibodies at the membrane confirmed successful translocation of the protein's N terminus across the membrane, with over 85% of the mNG-positive GUVs displaying concurrent antibody binding (Fig. 1*H*). The fluorescence recovery after photobleaching (FRAP) analysis further indicated that the membrane proteins are mobile in the phospholipid membrane (Fig. 2*I*), with a fluorescence recovery rate closely matching the diffusion kinetics of membrane proteins in GUVs reported in previous studies. These results gave critical evidence for the dynamic similarity between the membrane proteins synthesized via the membrane-proximal translation and their native counterparts. We encapsulated presynthesized subunit a, which had been produced in the absence of membranes using chol-ssDNA–modified complex as a negative control. As expected, these preformed hydrophobic products exhibited minimal association with the GUV membranes and showed no evidence of proper insertion (*SI Appendix*, Fig. S4). This experiment establishes the boundary condition that posttranslational exposure to membranes is insufficient for integration. Efficient membrane insertion therefore requires cotranslational folding in immediate contact with the lipid bilayer, as achieved by our membrane-anchored translation platform.

DNA Initiated Membrane Protein Expresses in Synthetic Cells. We have demonstrated efficient integration of protein membranes by employing presynthesized, purified mRNA to construct the membrane-anchored systems through hybridization with the chol-ssDNA. Natural cells utilize DNA-based transcription–translation cascades for rapid and regulated protein synthesis. To overcome the challenges, we developed a DNA-initiated system that mimics the central dogma, enabling de novo membrane protein synthesis from DNA templates with minimal external intervention. We coencapsulated chol-ssDNA, Cy3-ssDNA, and DNA templates with the PURE system into GUVs. The workflow includes: 1) the postencapsulation membrane anchoring of the chol-ssDNA; 2) the sequence-specific hybridization of the in situ transcribed nascent mRNA and the membrane-anchored chol-ssDNA; and 3) the membrane-proximal mRNA translation (Fig. 2*A*). The imaging of the dual-labeled Cy3-ssDNA-chol confirmed rapid membrane binding after the encapsulation (*SI Appendix*, Fig. S5). The time lapse fluorescence imaging revealed a dynamic redistribution process: The Cy3-ssDNA signals progressively shifted from the lumen to the membrane during the transcription, indicating continuous mRNA synthesis and targeted membrane anchoring. Correspondingly, the GFP-tagged proteins exhibited time-dependent accumulation on the membrane, while the fluorescence in the lumen remained at the background level, confirming spatially restricted translation near the membrane (*SI Appendix*, Fig. S6).

We systematically optimized the concentration of the chol-ssDNA as it was previously reported that high cholesterol content in lipid membranes might negatively impact the integration of membrane proteins. Our dose-dependent analysis revealed that the mRNA–membrane binding efficiency increased with the chol-ssDNA level, while the membrane protein integration reached saturation at 1 μM chol-ssDNA (Fig. 2 *B* and *C*)—a level well below the threshold typically associated with any perturbation of lipid organization or membrane protein behavior (45). The estimated membrane protein density under optimal conditions was approximately 1,200 proteins/μm^2, comparable to physiological densities of individual functional membrane proteins (Fig. 2*D*) (46). We observed a strong linear correlation between the mRNA localization efficiency and the membrane protein integration across all concentrations tested (slope k = 0.9, R^2 = 0.95), validating the spatial coupling mechanism (Fig. 2*E*).

Downloaded from https://www.pnas.org by CAS CONSORTIUM CHINESE ACADEMY OF SCIENCES on January 21, 2026 from IP address 159.226.35.236.

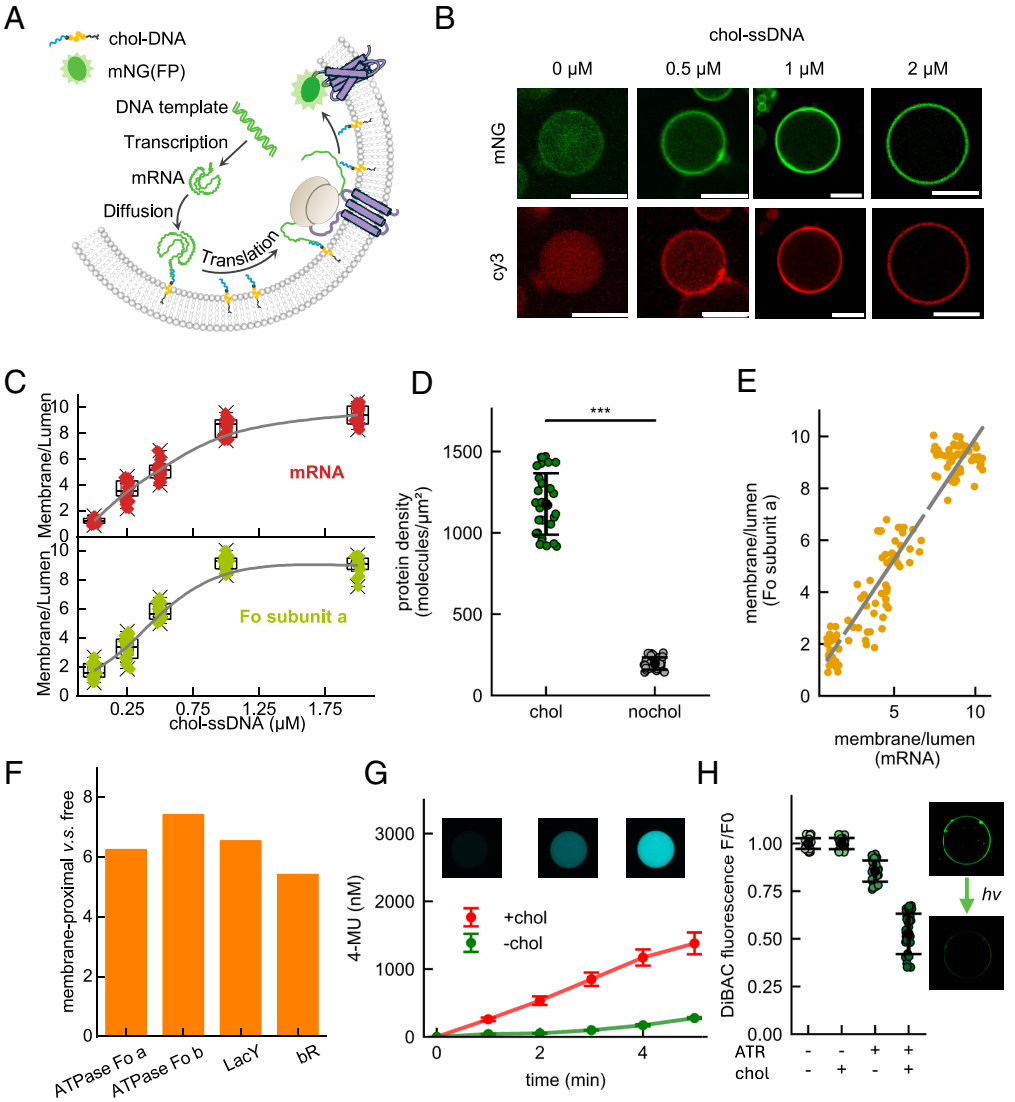

Fig. 2. Membrane proteins synthesized in GUVs via PURE from DNA. (*A*) Schematic illustrating the synthesis of membrane proteins within cell-sized GUVs. mRNA transcribed from DNA diffuses to the membrane and spontaneously binds to cholesterol-labeled ssDNA on the membrane, followed by translation in the vicinity of the membrane. (*B*) Representative images of Fo subunit a synthesized in GUVs encapsulating different concentrations of chol-ssDNA after 3 h of synthesis. (*C*) Quantification of membrane/lumen fluorescence intensity ratio derived from the radial profiles of mRNA fluorescence emission (*Up*) and mNG (*Down*) in individual GUVs. (*D*) Quantitative estimation of membrane protein density under optimal conditions, averaged from 30 GUVs of similar size (d = 20 μm). (*E*) Plot of the relationship between the membrane/lumen fluorescence intensity ratios of protein and mRNA in GUVs. (*F*) Quantification of membrane localization efficiencies for multiple proteins synthesized using the engineered membrane-proximal translation system. (LacY: lactose permease from *E. coli* MG1655; bR: bacteriorhodopsin from *Halobacterium halobium*). (*G*) Functional assay of LacY-mediated substrate transport in GUVs. (*H*) Light-driven proton-pumping activity of bR analyzed by membrane potential imaging.

To further validate the generalizability of our membrane-proximal translation system, we tested a variety of membrane proteins with distinct structural features, including those containing different numbers of transmembrane helices [e.g., bR with 7 helices and lactose permease (LacY) with 12 helices]. To minimize variability in total protein synthesis among individual GUVs, we used the membrane-to-lumen fluorescence ratio as a normalized indicator of membrane integration efficiency. As shown in Fig. 2*F*, all tested proteins exhibited several-fold higher membrane localization compared to the corresponding conditions without cholesterol-assisted anchoring. For LacY, we employed an optimized membrane composition with rich anionic and non–bilayer-forming lipids (DOPC: DOPE: DOPG = 4:4:2). 4-Methylumbelliferyl β-D-galactopyranoside (MUG) is transported by LacY and hydrolyzed by the β-galactosidase encapsulated inside GUVs to produce the fluorescent product 4-Methylumbelliferyl (4-MU). 4-MU fluorescence was converted to absolute concentrations using a calibration curve (*SI Appendix*, Fig. S7), enabling quantification of the accumulation rate (Fig. 2*G*). Based on the total number of membrane-localized LacY molecules and previously reported turnover rates for MUG (47, 48), we estimate that ~46% of these LacY molecules are correctly folded and functional. For bR, correct folding enables binding of its ligand all-trans retinal (ATR). Upon illumination, ATR-bound bR pumps protons outward, leading to a decrease in membrane potential. This change can be detected using the voltage-sensitive dye $DiBAC_4(3)$, as a drop in membrane potential reduces the reversible partitioning of the dye into the lipid bilayer and consequently decreases membrane fluorescence. When mRNA anchoring was omitted (chol–), only a weak response was observed—approximately 2 to 3 times lower than that of the anchored condition(chol+). Thus, anchoring the mRNA increases the absolute number of folded, ATR-bound, and functionally active bR molecules (Fig. 2*H*). Together, these results demonstrate that our DNA-initiated platform enables the

Downloaded from https://www.pnas.org by CAS CONSORTIUM CHINESE ACADEMY OF SCIENCES on January 21, 2026 from IP address 159.226.35.236.

synthesis of correctly folded and functional membrane proteins, with a translation-to-membrane coupling mechanism that is lipid-independent yet adaptable to diverse membrane compositions and protein architectures.

Expression of Dimeric Membrane Proteins in Synthetic Cells. While native cells rely on transmembrane proteins that precisely orchestrate their oligomerization to perform essential physiological functions, synthetic cells still face challenges in achieving bottom–up reconstitution of such higher-order membrane protein assemblies. Building on results above, we next sought to synthesize small dimeric membrane proteins. As a model, we selected EmrE, a multidrug transporter from *Escherichia coli* consisting of 110 amino acids and four transmembrane domains. The EmrE proteins function as antiparallel dimers in the membrane (49–51) (*SI Appendix*, Fig. S8). Due to its small size, dual topology, and high hydrophobicity, EmrE has been reported to appear in the insoluble fraction when synthesized using in vitro translation. Notably, substantial increase in the integration efficiency was reportedly achieved by reducing the size of the synthetic cells, thereby increasing the phospholipid concentration around the translation machinery (24). Here, anchoring the mRNA to the membrane provides a versatile approach to produce membrane proteins in synthetic cells without restricting their size.

We employed the transmembrane dye FlAsH, which covalently binds to the tetracysteine tag (TC-Tag) and generates fluorescence, to track the localization and ratio of the EmrE protein during in vitro synthesis. We avoided using fluorescent proteins like GFP, as the large size of GFP might disrupt EmrE's dimerization and topological inversion. We synthesized the mRNA encoding EmrE with a TC-tag and an AnchorTail sequence. Translation experiments on SLBs demonstrated that this approach supports EmrE synthesis and dimerization. We used single-molecule photobleaching step analysis to quantify the subunit number within the protein complexes. The stepwise photobleaching events indicated the formation of a dimeric structure (*SI Appendix*, Fig. S8). To assess the membrane integration efficiency and functionality of the synthesized EmrE transporter, we conducted systematic analyses using the previously described DNA template system. Prior studies have reported suboptimal membrane integration efficiency (<1%) for EmrE in synthetic cells of this size range (24). In line with this, our control experiments (Fig. 3*A*) without the cholesterol-modified ssDNA revealed no significant difference in fluorescence between the membrane and the lumen of the synthetic cell. Remarkably, the recruitment of the AnchorTail sequence-containing mRNA by the cholesterol-tagged ssDNA enhanced significantly the membrane-localized proportion of EmrE, as evidenced by a sixfold increase in the membrane-to-lumen fluorescence ratio compared to that in the control experiments (Fig. 3*B*).

To evaluate the transport activity of the synthesized EmrE oligomers, we used ethidium bromide (EtBr)—a fluorescent substrate that intercalates with nucleic acids—as a model for substrate-selective uptake (Fig. 3*C*). Following EmrE expression in GUVs, we established a transmembrane pH gradient and added EtBr to the external medium. Fluorescence imaging revealed marked accumulation of EtBr within the EmrE-expressing GUVs, whereas control vesicles—either empty or expressing a nonfunctional protein—showed no detectable EtBr entry, thereby excluding the passive leakage as the source of the observed signal (*SI Appendix*, Fig. S9). Quantitative analysis of the transport kinetics revealed superior performance in cholesterol-modified systems, with the EtBr influx rate in the experimental group surpassing the controls (Fig. 3 *D* and *E*). We posit that the difference in the selective uptake arises from difference in the amounts of

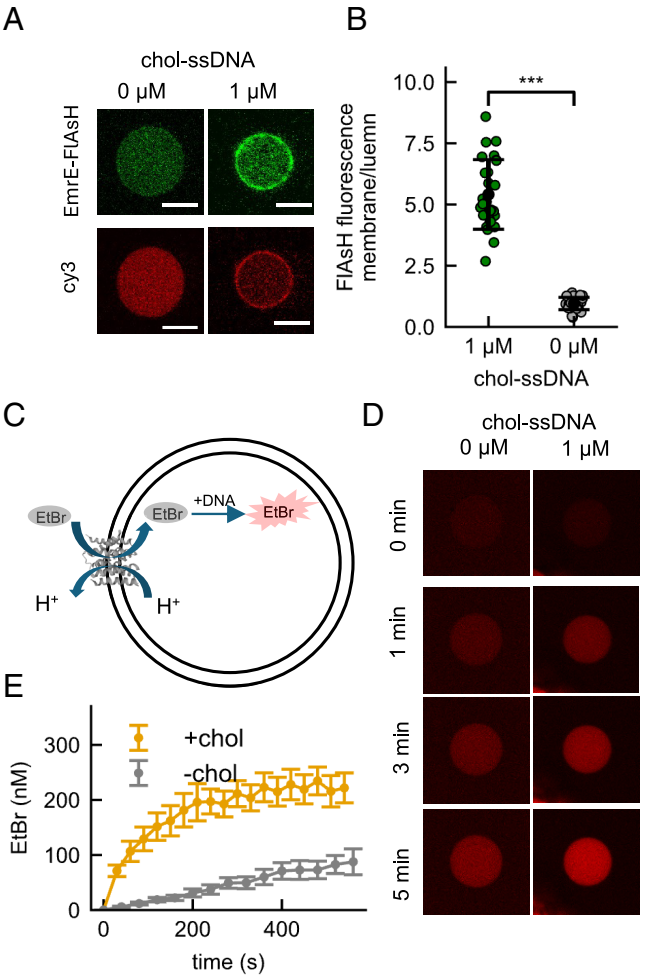

Fig. 3. Expression of dimeric membrane proteins and selective uptake of substrates in large synthetic cells. (*A*) Typical GUV image. Green fluorescence indicates the FlAsH-labeled EmrE, and red fluorescence indicates the cy3-labeled mRNA. (*B*) Quantification of the FlAsH fluorescence intensity from a single GUV. Mean value (open square), median, and quartiles are shown for 26 individual GUVs for both conditions. Statistical significance was analyzed via one-way ANOVA with Tukey [HSD] post hoc analysis, ***$P < 0.001$. (*C*) Schematic of EtBr transport by EmrE and fluorescence-based functional assay of EmrE. (*D*) Representative microscopy images of EmrE transporting EtBr into a GUV. (*E*) The corresponding EtBr in GUV as a function of time. The normalized fluorescence intensity of EtBr/DNA was calculated from three independent samples. The data were presented as the mean values ± SDs; n = 3 independent replicates.

the membrane proteins. Comparison of the measured EtBr initial uptake rate (29.8 nmol min^{-1} mg^{-1}) with the reported turnover rate of EmrE (52) indicates that ~49% of membrane-localized EmrE was correctly folded and active. These findings confirm the successful membrane integration of functional EmrE transporters and support their operation as antiparallel homodimers.

Spatial mRNA Organization Programs Membrane Protein Stoichiometry. We have observed a strong positive correlation between the number of the membrane-anchored mRNAs and the expression levels of the integral membrane proteins in the synthetic cells (Fig. 2*E*). It suggests that the spatial organization of the mRNA can be harnessed to regulate the membrane protein stoichiometry. To test this, we developed a programmable mRNA anchoring strategy that encodes spatial information into the 3′UTRs of the target mRNA. Specifically, orthogonal anchoring sequences (Anchor-A or Anchor-B) were appended to the mRNAs, enabling sequence-specific hybridization to the cholesterol-tagged

Downloaded from https://www.pnas.org by CAS CONSORTIUM CHINESE ACADEMY OF SCIENCES on January 21, 2026 from IP address 159.226.35.236.

ssDNA probes (chol-ssDNA-A/B) pretethered on the membrane. By varying the molar ratio of the membrane-tethered probes, we tuned the local density of each mRNA species and, in turn, modulated membrane protein expression ratios (Fig. 4*A*). To isolate the effect of mRNA localization from differences in transcription, translation, or folding, we designed a two-color reporter system using identical protein sequences fused to distinct fluorescent proteins—mNeonGreen (mNG) or mScarlet (mS)—and different anchors. DNA templates (atpB–mNG–Anchor-A and atpB–mS–Anchor-B) were cotranscribed, and the ratio of membrane-bound chol-ssDNA-A to chol-ssDNA-B was systematically varied. Quantitative analysis (*SI Appendix*, Fig. S10) of the confocal images revealed a linear relationship between the membrane expression ratio of the two reporters and the corresponding probe ratio (*SI Appendix*, Fig. S11), demonstrating that spatial mRNA anchoring enables tunable and predictable control of membrane protein stoichiometry.

We next asked whether this strategy could be extended to directly control stoichiometric ratios of subunits within a multisubunit membrane protein. Achieving precise stoichiometric assembly of multisubunit membrane proteins remains a major challenge in synthetic biology. Conventional approaches typically rely on modulating the input concentration of the DNA templates for each subunit. While effective to some degrees, this approach is inconsistent with the genomic stability of natural cells, where the DNA copy number is relatively fixed. Our spatial anchoring method, by contrast, allows the decoupling of the subunit stoichiometry from the DNA dosage by controlling mRNA localization directly at the membrane. As a case study, we focused on the Fo complex of the ATP synthase, in which the a-subunit (encoded by atpB) and b-subunit (encoded by atpF) are expressed at a defined stoichiometric ratio of 1:2. We applied our system to coexpress both subunits from the DNA templates held at equal concentrations (20 nM) and varied only the ratio of chol-ssDNA-A to chol-ssDNA-B in the membrane (ranging from 3:0 to 0:3) (Fig. 4 *B* and *C*). This strategy resulted in precise control over the relative expression levels of the two subunits. Remarkably, even when the DNA template input ratios were deliberately perturbed (Fig. 4*D*), the protein output ratio remained stable so long as the membrane probe ratio was fixed (Fig. 4 *E* and *F*). We further extended this strategy to the Fo subunit c and confirmed its membrane integration and correct topology by immunofluorescence. We used FlAsH staining to quantify the total population of membrane-localized Fo-c, while external epitope accessibility assays selectively measured the subset of molecules whose C-terminal tags were exposed to the vesicle exterior. Integrating these two measurements showed that approximately 77% of membrane-associated Fo-c adopts the correct outward-facing topology (*SI Appendix*, Fig. S12). Although full Fo assembly in vivo involves specific insertases and lipid components, our

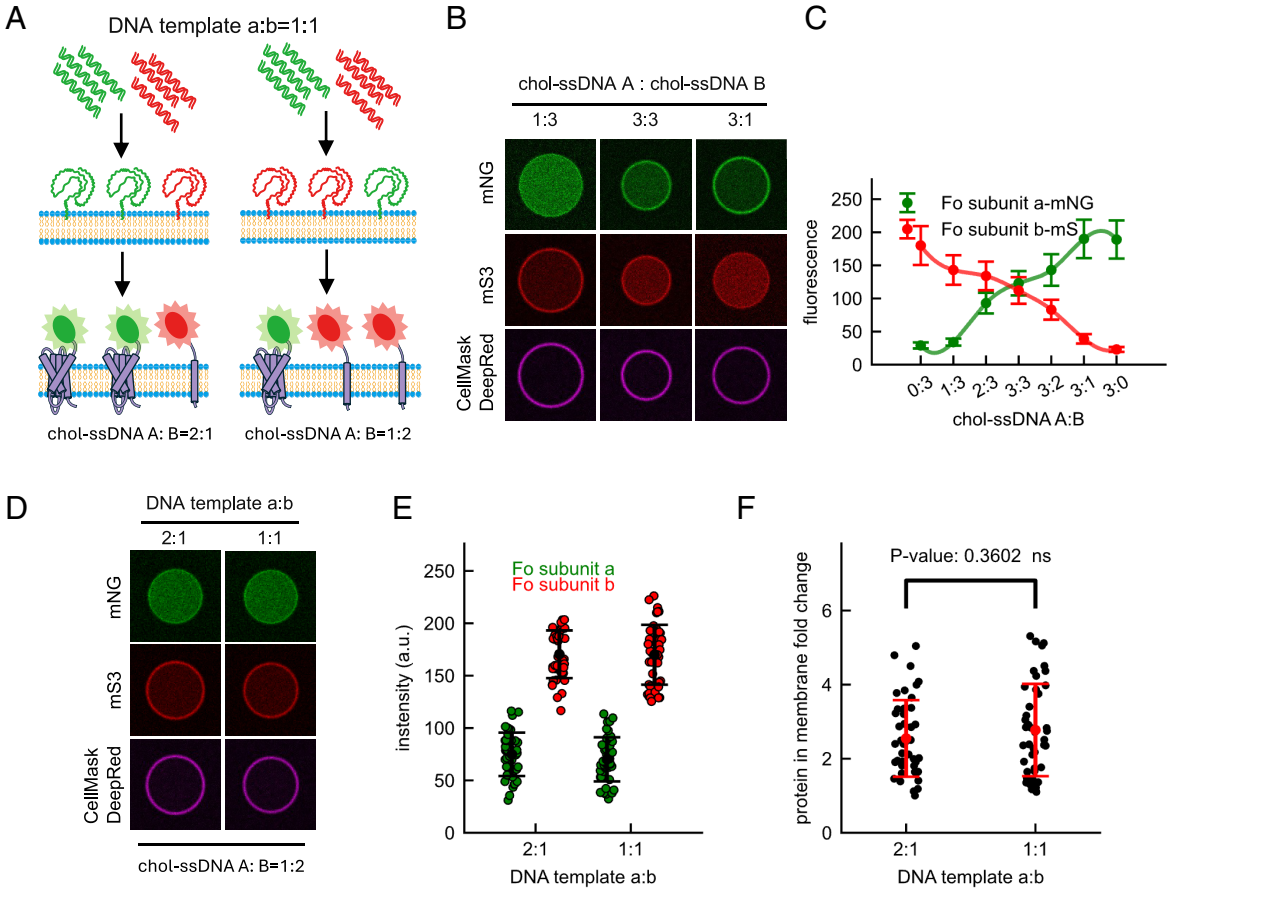

Fig. 4. Decoupling DNA template input from protein output via membrane-anchored mRNA translation. (*A*) Schematic illustrating control of membrane protein stoichiometry by varying the ratio of cholesterol-modified ssDNA A to ssDNA B. (*B*) Representative confocal fluorescence images corresponding to (*A*). mNG indicates the Fo subunit a; mS3 indicates the Fo subunit b; CellMask DeepRed stains the phospholipid bilayer. (*C*) Quantification of membrane-localized fluorescence intensities under varying chol-ssDNA A:B ratios (n > 25 GUVs per condition). Fluorescence intensities were normalized based on prior calibration between protein concentration and fluorescence using a fluorometer. Error bars represent one SD. (*D*) Representative confocal fluorescence images showing modulation of membrane protein stoichiometry by varying DNA template ratios, while maintaining a constant chol-ssDNA A:B ratio. (*E*) Quantification of membrane-localized fluorescence intensities under varying DNA template ratios (n > 40 GUVs per condition). (*F*) Fluorescence intensity ratio of mS3 to mNG on individual GUV membranes, used to infer the stoichiometric ratio of Fo subunit b to Fo subunit a.

Downloaded from https://www.pnas.org by CAS CONSORTIUM CHINESE ACADEMY OF SCIENCES on January 21, 2026 from IP address 159.226.35.236.

results highlight that spatially guided mRNA translation enables stoichiometrically controlled synthesis and membrane integration of individual subunits.

Altogether, this approach effectively decouples gene dosage from protein abundance, bringing synthetic cells closer to the regulatory logic of natural systems—where a stable genome underlies dynamic proteomic responses—and establishes a foundational framework for building functionally programmable synthetic life systems.

Discussion

This study presents a novel strategy for spatially confining mRNA near the synthetic cell membranes by engineering the 3'UTRs. By incorporating chol-ssDNA recognition motifs into the 3'UTR, we achieved membrane-proximal translation in GUVs. This localized translation facilitates both cotranslational folding and the integration of membrane proteins. Our quantitative analyses revealed a 6- to 10-fold increase in the membrane integration efficiency as compared to the free mRNA-based controls. Notably, for the proteins examined in this study, we estimate that approximately 40 to 80% of the membrane-localized protein population adopts the correct folding. More importantly, we achieved the high-efficiency selective substrate uptake and the decoupling of the DNA template dosage from the membrane protein production in synthetic cells.

Membrane proteins, enriched in hydrophobic amino acid residues, pose significant challenges for synthesis and folding in aqueous environments. While natural cells rely on dedicated pathways such as the SRP–SEC translocon (Fig. 1*A*), synthetic systems confront two major limitations: precise control over stoichiometric coexpression and difficulty in reconstituting complex multisubunit membrane assemblies like SecYEG and Sec61. Inspired by the liposome cell-free (L-CF) model—which enhances the hydrophobic peptide–lipid interactions by increasing the concentration of the liposome—conventional synthetic strategies often rely on reducing the liposome size to minimize the diffusion distance between the translation machinery and the membrane. Our platform circumvents this size limitation by recruiting ribosomes to membrane-tethered mRNAs, ensuring that the translation occurs within molecular-scale distances of the membrane. Unlike traditional optimization-based approaches, our sequence-programmable strategy is broadly applicable across diverse membrane protein types and requires no modification of the coding sequence (CDS). We enabled efficient synthesis and integration of membrane proteins with varying numbers of transmembrane helices and oligomeric configurations. Although the current implementation utilizes chol-ssDNA for mRNA anchoring, the framework is compatible with alternative tethering strategies, such as the 3' UTR-binding proteins or synthetic ligands. This modular design supports spatially resolved expression: Membrane proteins are translated at membrane surfaces, while cytoplasmic proteins are synthesized in solution, effectively recapitulating subcellular compartmentalization.

While validated in GUVs for the expression of plasma membrane-associated proteins, this approach holds broad potential for synthetic biology. By leveraging programmable 3'UTR–mediated hybridization, the ability to program spatially resolved gene expression via 3'UTR engineering could reshape the design of synthetic cells, particularly for systems requiring precise membrane protein localization, such as synthetic photosynthetic platforms or biosensing interfaces. Furthermore, the observed correlation between mRNA localization, translation efficiency, and protein integration provides a quantitative framework for optimizing synthetic cell architectures. While our system enables DNA-initiated synthesis and membrane integration of multiple protein subunits, the coordinated assembly of large multicomponent complexes remains technically challenging. Such assemblies typically depend on tightly regulated hierarchical pathways, lipid microdomain organization, and transient chaperone assistance that couple subunit folding with membrane insertion. By contrast, simpler oligomeric complexes such as the dimeric transporter EmrE can form spontaneously through diffusion-driven encounters, illustrating that our platform intrinsically supports the formation of correctly folded and functionally inserted membrane proteins. Looking ahead, the integration of orthogonal anchoring systems could enable multiplexed spatial control of distinct protein populations within a single chassis, accelerating the bottom–up assembly of functionally sophisticated synthetic cells. By bridging minimalist design with functional complexity, this platform advances the construction of synthetic cells capable of environmentally responsive behaviors, and provides a foundation for the development of biosensors, artificial signaling networks, and self-sustaining synthetic cellular systems.

Materials and Methods

All phospholipids were purchased from Avanti Polar Lipids. The in vitro transcription kit (M0251S) was obtained from New England Biolabs (NEB). The PURE system (PURExpress® 2.1) was sourced from GeneFrontier. Unless otherwise noted, DNA and RNA oligonucleotides were synthesized by Sangon Biotech, and chemicals were obtained from Sigma-Aldrich.

Preparation of Template DNA and mRNA. Plasmids encoding Fo subunit a (atpB), Fo subunit b (atpF), LacY, EmrE, and bacteriorhodopsin (bR)–namely pET28-atpB-mNG, pET28-atpB-mS, pET28-LacY-mNG, pET28-EmrE-TcTag, and pET28-bR-sfGFP–were commercially synthesized by BGI. Each construct includes a T7 promoter and ribosome-binding site (RBS). Template DNA was PCR-amplified with tag and AnchorTail sequences (primer sequences listed in *SI Appendix*, Table S1) and verified by sequencing. In vitro transcription was carried out using a T7 RNA polymerase system. IVT reactions (100 μL) were diluted in 900 μL Tris-HCl buffer (pH 7.5), extracted with 200 μL chloroform, and RNA was precipitated with isopropanol and sodium acetate. Pellets were washed with 75% ethanol, resuspended in RNase-free water, and stored at −80 °C.

Chol-ssDNA/mRNA in Supported Lipid Bilayer (SLB) and TIRF Microscopy. Small unilamellar vesicles (SUVs) composed of 1-palmitoyl-2-oleoyl-sn-glycero-3-phosphocholine (POPC) were prepared at a concentration of 2 mg/mL via the thin-film hydration method. Briefly, POPC dissolved in chloroform was evaporated under a nitrogen stream, dried under vacuum, and hydrated with 5 mL of PBS (prepared with Milli-Q water) at 37 °C. The suspension was sonicated until optically clear. SLBs were formed by depositing 80 μL of the SUV solution onto thoroughly cleaned glass coverslips, followed by a 6-h incubation period and subsequent rinsing with PBS. Single-molecule imaging was performed using a custom-built objective-type TIRF microscope, with wavelength settings optimized for specific fluorophores. Annealed mRNA was diluted and introduced into poly (methyl methacrylate) wells containing SLBs for real-time imaging.

Cell-Free Protein Synthesis in GUV. GUVs were generated using the water-in-oil (w/o) emulsion transfer method. The inner phase consisted of 20 μL PURE system supplemented with template DNA, 200 mM sucrose, 0.8 U/μL RNase inhibitor, 50 nM Cy3-labeled ssDNA, and cholesterol-modified (or unmodified) ssDNA. This mixture was vortexed with 600 μL mineral oil containing 0.5 mg/mL POPC for 30 s, then incubated on ice for 10 min. Subsequently, 600 μL of this emulsion was layered over 200 μL of outer solution and centrifuged at 2,000 g for 10 min at 4 °C. GUVs were harvested from the tube bottom and suspended in fresh outer solution. Protein expression was carried out at 37 °C for 3 h. The outer solution contained the low-molecular-weight components of the PURE system and 200 mM glucose for osmotic balance but lacked ribosomes and translation machinery.

Estimation of Membrane Protein Copy Number. To estimate the surface density of membrane-associated proteins in GUVs, we established a geometric relationship between fluorescence intensity and molecular density under confocal

Downloaded from https://www.pnas.org by CAS CONSORTIUM CHINESE ACADEMY OF SCIENCES on January 21, 2026 from IP address 159.226.35.236.

imaging. For a vesicle of radius R, let the membrane-associated fluorophore surface density be ρ (molecules μm^{-2}) and the fluorophore concentration in the lumen be c. Assuming the confocal point spread function (PSF) can be approximated by a cube of side length d (full width at half maximum), the ratio between the peak fluorescence intensity at the membrane (I_{mem}) and that at the center of the vesicle (I_{lumen}) can be expressed as:

$$\frac{I_{mem}}{I_{lumen}} \approx 1 + \frac{\rho}{c\,d\,N_A},$$

where N_A denotes Avogadro's constant.

This relationship allows quantitative estimation of the membrane surface density ρ from confocal fluorescence data when the internal concentration c and PSF width d are known. The linear relationship between fluorescence intensity and fluorophore concentration (c) was readily established using purified fluorescent proteins under identical imaging conditions. To obtain accurate calibration parameters, defined molar fractions of Cy5–phosphatidylethanolamine (Cy5-PE) were incorporated into lipid membranes to generate vesicles with known fluorescent surface densities. Under identical imaging conditions, the fluorescence intensity–concentration calibration was performed to determine the PSF factor width d (≈180 nm, *SI Appendix*, Fig. S2). These parameters were then used to quantitatively estimate the membrane molecular density from confocal fluorescence images.

Immunofluorescent Detection of Exposed Protein Epitopes. To assess the exposure of protein epitopes on the exterior surface of GUVs, we performed immunofluorescence labeling on two constructs: i) N-terminally FLAG-tagged Fo subunit a and ii) C-terminally myc-tagged Fo subunit c. For FLAG-tagged samples, an Alexa Fluor® 647-conjugated anti-FLAG antibody was added to the vesicle suspension at a final concentration of 5 μg/mL and incubated at 37 °C for 30 min. For myc-tagged samples, an Alexa Fluor® 488 conjugated anti-myc antibody was used under identical labeling conditions. After incubation, unbound antibodies were removed by pelleting the GUVs at 2,000 g for 5 min, followed by gentle resuspension of the pellet in dilution buffer. The labeled GUVs were subsequently analyzed by confocal fluorescence microscopy to evaluate the accessibility of the corresponding external epitopes. Quantitative analysis of epitope exposure was performed following the general approach described previously (24), with minor modifications to account for the calibrated confocal PSF (*SI Appendix*, Fig. S2). Briefly, the fluorescence intensity along the GUV membrane was extracted and compared with a standard fluorescence–concentration calibration obtained for the corresponding fluorescent antibodies. By combining the measured membrane fluorescence with the PSF-corrected surface intensity model, we estimated the number of accessible epitopes per vesicle. This analysis enabled quantification of the fraction of correctly folded and outward-facing proteins in each construct.

Selective Nuclease Digestion of External Nucleic Acids. GUVs containing the mRNA:chol-ssDNA:Cy3-ssDNA complexes were prepared by the inverse emulsion method as described above. After vesicle formation, the suspension was divided into two portions: One was kept as an untreated control, and the other was subjected to nuclease digestion to remove nucleic acids located on the outer membrane surface. For digestion, vesicles were incubated with 100 U/μL Benzonase Nuclease and 5 μg/mL RNase A at 37 °C for 30 min. Following treatment, GUVs were transferred into microscopy chambers and allowed to sediment at room temperature for 15 to 20 min prior to confocal imaging. Identical imaging parameters were applied to both treated and untreated samples. Membrane fluorescence intensities were quantified from the radial fluorescence profiles of individual vesicles before and after digestion to assess the relative contributions of external and internal nucleic acids.

Functional Validation of LacY. To evaluate transport activity, β-galactosidase (β-gal, Sigma-Aldrich) was pre-encapsulated in the internal solution during GUV formation at a final concentration of 0.5 mg mL^{-1}. Before fluorescence measurement, MUG, (20 μM) was added to the external buffer, defining time zero for substrate exposure. Fluorescence images were acquired at defined time intervals using confocal microscopy with 405 nm excitation and 420 to 460 nm emission detection under identical imaging settings. The mean fluorescence intensity within individual vesicles was quantified at each time point, and transport activity was evaluated based on the relative increase in intravesicular 4-MU fluorescence over time. Fluorescence intensities were converted to absolute 4-MU concentrations using the calibration curve described in *SI Appendix*, Fig. S7. The total number of LacY molecules per vesicle (N) was estimated from the membrane molecular density measured in Fig. 2*D*. Dividing the total transport rate by N yielded the apparent turnover number per LacY molecule. Comparison of this value with reported turnover numbers for purified LacY reconstituted in liposomes allowed us to estimate the fraction of correctly folded and functional LacY in our system.

Functional Validation of bR by $DiBAC_4(3)$ Fluorescence Assay. GUVs containing the PURE system were prepared as described above and incubated at 37 °C in the dark for 3 h to allow in situ protein synthesis. After expression, vesicle suspensions were cooled to 4 °C and supplemented with 1 μM $DiBAC_4(3)$. Samples were transferred to microscopy chambers and kept in the dark for 20 min to allow vesicle sedimentation before imaging. For membrane-potential measurements, vesicles were continuously illuminated with a 561 nm laser for 300 s, which excites bR but does not interfere with $DiBAC_4(3)$ fluorescence. Illumination was immediately followed by fluorescence imaging of membrane-associated $DiBAC_4(3)$ using 488 nm excitation under identical acquisition settings. The fluorescence intensity of the membrane region was quantified, and the relative change ($\Delta F/F_0$) was used to evaluate light-induced potential formation.

FlAsH Staining of Membrane-Associated Proteins in GUVs. After protein expression, GUV suspensions were equilibrated to room temperature, and FlAsH-EDT_2 was added to a final concentration of 100 nM. Samples were incubated for 30 min at room temperature in the dark to allow specific binding of FlAsH to the TC motif. Excess dye was removed by pelleting the GUVs at 2,000 g for 5 min and gently resuspending the pellet in fresh dilution buffer supplemented with 1 mM BAL to minimize nonspecific background. The FlAsH-labeled GUVs were imaged by confocal fluorescence microscopy using 488 nm excitation under identical acquisition settings for all samples. GUVs prepared with a PURE reaction lacking the DNA template were processed in parallel and used as background controls; this background fluorescence was subtracted during quantitative analysis. Membrane fluorescence intensities extracted from confocal images were converted into the total number of membranes associated proteins using a fluorescence–concentration calibration curve established for FlAsH labeled TC peptide.

EtBr Uptake Experiments. For EtBr uptake experiments, GUVs containing the PURE system were prepared as described above and incubated at 37 °C for 3 h to allow in situ synthesis of EmrE. To initiate transport, the external buffer was replaced with dilution buffer containing 10 μM EtBr (pH 8.1), defining time zero for substrate exposure. EtBr is intrinsically fluorescent upon binding to nucleic acids, enabling direct visualization of substrate accumulation inside GUVs. Fluorescence images were acquired at defined time intervals using confocal microscopy with 488 nm excitation and 560 to 620 nm emission detection under identical imaging conditions. Image analysis was performed in ImageJ. The mean intravesicular fluorescence of individual GUVs was quantified over time, and EtBr uptake was evaluated based on the increase in internal fluorescence relative to background. To obtain quantitative transport rates, EtBr fluorescence intensities were converted into absolute EtBr concentrations using a standard calibration curve. The radius of each GUV was used to estimate its internal volume, allowing calculation of the total number of EtBr molecules imported per vesicle. Following the analysis strategy used previously for EmrE, the measured EtBr uptake rate was compared with the reported turnover rate of EmrE for EtBr (61 nmol min^{-1} mg^{-1} for 10 μM EtBr) to estimate the number of functional EmrE dimers present in the GUV membrane.

Protein Expression and Purification. The plasmids containing mNeonGreen and mScarlet on pRSETA vector were transfected into BL21(DE3) competent cell and plated onto the LB culture medium (supplemented with 100 μg/mL Amp). The next day, one single clone was picked into 2 mL liquid LB medium for overnight culture. One milliliter of bacteria was transferred to 200 mL culture medium in a 500 mL flask and continued to cultivate until OD600 = 0.8. Protein expression was induced by IPTG (final concentration 0.8 mM) at 16 °C for 20 h. Cells were collected by centrifugation, resuspended in the Ni-column binding buffer (20 mM imidazole, 500 mM NaCl, 50 mM NaH2PO4) supplemented with 1 mg/mL lysozyme, 1 mM PMSF, 1× protease inhibitors (Beyotime Biotechnology, China), and lysed by ultrasonication (work 3 s and stop 5 s). Proteins were purified by Ni-NTA His-Bind resin (Qiagen, Germany) followed by gel filtration (Superdex 200, GE Healthcare) at 4 °C and stored in PBS at −80 °C for further analysis.

Downloaded from https://www.pnas.org by CAS CONSORTIUM CHINESE ACADEMY OF SCIENCES on January 21, 2026 from IP address 159.226.35.236.

Confocal Microscopy. Images were captured using an Olympus FV3000 confocal microscope. Fiji software was used for fluorescence image analysis, with background adjustments made using predefined ROIs near each GUV.

Statistical Analysis. Data were analyzed using one-way ANOVA with Tukey's post hoc test and two-tailed, two-sample Student's *t* test, performed using Python version 3.10. Statistical significance was assumed for *P*-values < 0.001 unless stated otherwise.

Data, Materials, and Software Availability. Study data are included in the article and/or *SI Appendix*.

ACKNOWLEDGMENTS. This work was supported by the Strategic Priority Research Program of the Chinese Academy of Sciences XDB0480000. National Key Research and Development Programme of China 2019YFA0709304. Chinese Academy of Sciences Project for Young Scientists in Basic Research YSBR-104 National Natural Science Foundation of China T2221001. National Natural Science Foundation of China 32171228. National Natural Science Foundation of China 32471278. China Postdoctoral Science Foundation 2024M763506.

Author affiliations: [a]Beijing National Laboratory for Condensed Matter Physics, Institute of Physics, Chinese Academy of Sciences, Beijing 100190, China; [b]Wenzhou Institute, University of Chinese Academy of Sciences, Wenzhou, Zhejiang 325000, China; [c]University of Chinese Academy of Sciences, Beijing 100049, China; [d]Key Laboratory of Quantitative Synthetic Biology, Shenzhen Institute of Synthetic Biology, Shenzhen Institutes of Advanced Technology, Chinese Academy of Sciences, Shenzhen 518055, China; and [e]Beijing National Laboratory for Molecular Sciences, Laboratory of Polymer Physics and Chemistry, CAS Research/Education Center for Excellence in Molecular Sciences, Institute of Chemistry, Chinese Academy of Sciences, Beijing 100190, China

1. E. Rideau, R. Dimova, P. Schwille, F. R. Wurm, K. Landfester, Liposomes and polymersomes: A comparative review towards cell mimicking. *Chem. Soc. Rev.* **47**, 8572–8610 (2018).
2. L. J. Rothschild *et al.*, Building synthetic cells—From the technology infrastructure to cellular entities. *ACS Synth. Biol.* **13**, 974–997 (2024).
3. C. Monck, Y. Elani, F. Ceroni, Genetically programmed synthetic cells for thermo-responsive protein synthesis and cargo release. *Nat. Chem. Biol.* **20**, 1380–1386 (2024).
4. M. A. Yıldırım, K.-I. Goh, M. E. Cusick, A.-L. Barabási, M. Vidal, Drug–Target network. *Nat. Biotechnol.* **25**, 1119–1126 (2007).
5. S. Kohyama, A. Merino-Salomón, P. Schwille, In vitro assembly, positioning and contraction of a division ring in minimal cells. *Nat. Commun.* **13**, 6098 (2022).
6. K. Y. Lee *et al.*, Photosynthetic artificial organelles sustain and control ATP-dependent reactions in a protocellular system. *Nat. Biotechnol.* **36**, 530–535 (2018).
7. S. Berhanu, T. Ueda, Y. Kuruma, Artificial photosynthetic cell producing energy for protein synthesis. *Nat. Commun.* **10**, 1325 (2019).
8. N. De Franceschi, R. Barth, S. Meindlhumer, A. Fragasso, C. Dekker, Dynamin a as a one-component division machinery for synthetic cells. *Nat. Nanotechnol.* **19**, 70–76 (2024).
9. P. Girard *et al.*, A new method for the reconstitution of membrane proteins into giant unilamellar vesicles. *Biophys. J.* **87**, 419–429 (2004).
10. A. Varnier *et al.*, A simple method for the reconstitution of membrane proteins into giant unilamellar vesicles. *J. Membr. Biol.* **233**, 85–92 (2010).
11. J. S. Hansen *et al.*, Formation of giant protein vesicles by a lipid cosolvent method. *Chembiochem* **12**, 2856–2862 (2011).
12. M. Dezi, A. Di Cicco, P. Bassereau, D. Lévy, Detergent-mediated incorporation of transmembrane proteins in giant unilamellar vesicles with controlled physiological contents. *Proc. Natl. Acad. Sci. U.S.A.* **110**, 7276–7281 (2013).
13. R. R. Ishmukhametov, A. N. Russell, R. M. Berry, A modular platform for one-step assembly of multi-component membrane systems by fusion of charged proteoliposomes. *Nat. Commun.* **7**, 13025 (2016).
14. I. L. Jørgensen, G. C. Kemmer, T. G. Pomorski, Membrane protein reconstitution into giant unilamellar vesicles: A review on current techniques. *Eur. Biophys. J.* **46**, 103–119 (2017).
15. Y. Shimizu *et al.*, Cell-free translation reconstituted with purified components. *Nat. Biotechnol.* **19**, 751–755 (2001).
16. H. Matsubayashi, Y. Kuruma, T. Ueda, In vitro synthesis of the *E. coli* Sec translocon from DNA. *Angew. Chem. Int. Ed. Engl.* **53**, 7535–7538 (2014).
17. Y. Kuruma, T. Ueda, The PURE system for the cell-free synthesis of membrane proteins. *Nat. Protoc.* **10**, 1328–1344 (2015).
18. S. Wang *et al.*, The molecular mechanism of cotranslational membrane protein recognition and targeting by SecA. *Nat. Struct. Mol. Biol.* **26**, 919–929 (2019).
19. N. Ismail, R. Hedman, M. Lindén, G. von Heijne, Charge-driven dynamics of nascent-chain movement through the SecYEG translocon. *Nat. Struct. Mol. Biol.* **22**, 145–149 (2015).
20. J. Frauenfeld *et al.*, Cryo-EM structure of the ribosome–SecYE complex in the membrane environment. *Nat. Struct. Mol. Biol.* **18**, 614–621 (2011).
21. R. Steinberg, L. Knüpffer, A. Origi, R. Asti, H.-G. Koch, Co-translational protein targeting in bacteria. *FEMS Microbiol. Lett.* **365**, fny095 (2018).
22. I. L. Volkov *et al.*, Spatiotemporal kinetics of the SRP pathway in live *E. coli* cells. *Proc. Natl. Acad. Sci. U.S.A.* **119**, e2204038119 (2022).
23. D. Schibich *et al.*, Global profiling of SRP interaction with nascent polypeptides. *Nature* **536**, 219–223 (2016).
24. H. Soga *et al.*, In vitro membrane protein synthesis inside cell-sized vesicles reveals the dependence of membrane protein integration on vesicle volume. *ACS Synth. Biol.* **3**, 372–379 (2014).
25. R. Eaglesfield, M. A. Madsen, S. Sanyal, J. Reboud, A. Amtmann, Cotranslational recruitment of ribosomes in protocells recreates a translocon-independent mechanism of proteorhodopsin biogenesis. *iScience* **24**, 102429 (2021).
26. R. S. Hegde, R. J. Keenan, A unifying model for membrane protein biogenesis. *Nat. Struct. Mol. Biol.* **31**, 1009–1017 (2024).
27. J. A. Peruzzi *et al.*, Hydrophobic mismatch drives self-organization of designer proteins into synthetic membranes. *Nat. Commun.* **15**, 3162 (2024).
28. C. Meyer *et al.*, Designer artificial environments for membrane protein synthesis. *Nat. Commun.* **16**, 4363 (2025).
29. J. Steinkühler *et al.*, Improving cell-free expression of model membrane proteins by tuning ribosome cotranslational membrane association and nascent chain aggregation. *ACS Synth. Biol.* **13**, 129–140 (2024).
30. N. J. Harris, G. A. Pellowe, P. J. Booth, Cell-free expression tools to study co-translational folding of alpha helical membrane transporters. *Sci. Rep.* **10**, 9125 (2020).
31. J. Lawrence, Intracellular localization of messenger RNAs for cytoskeletal proteins. *Cell* **45**, 407–415 (1986).
32. S. Das, M. Vera, V. Gandin, R. H. Singer, E. Tutucci, Intracellular mRNA transport and localized translation. *Nat. Rev. Mol. Cell Biol.* **22**, 483–504 (2021).
33. E. Korkmazhan, H. Teimouri, N. Peterman, E. Levine, Dynamics of translation can determine the spatial organization of membrane-bound proteins and their mRNA. *Proc. Natl. Acad. Sci. U.S.A.* **114**, 13424–13429 (2017).
34. C. Xia, J. Fan, G. Emanuel, J. Hao, X. Zhuang, Spatial transcriptome profiling by MERFISH reveals subcellular RNA compartmentalization and cell cycle-dependent gene expression. *Proc. Natl. Acad. Sci. U.S.A.* **116**, 19490–19499 (2019).
35. S. Mili, K. Moissoglu, I. G. Macara, Genome-wide screen reveals APC-associated RNAs enriched in cell protrusions. *Nature* **453**, 115–119 (2008).
36. D. W. Reid, C. V. Nicchitta, Diversity and selectivity in mRNA translation on the endoplasmic reticulum. *Nat. Rev. Mol. Cell Biol.* **16**, 221–231 (2015).
37. E. Villanueva *et al.*, System-wide analysis of RNA and protein subcellular localization dynamics. *Nat. Methods* **21**, 60–71 (2024).
38. P. Sarmah *et al.*, mRNA targeting eliminates the need for the signal recognition particle during membrane protein insertion in bacteria. *Cell Rep.* **42**, 112140 (2023).
39. K. Nevo-Dinur, A. Nussbaum-Shochat, S. Ben-Yehuda, O. Amster-Choder, Translation-independent localization of mRNA in *E. coli*. *Science* **331**, 1081–1084 (2011).
40. X. A. Cui, H. Zhang, A. F. Palazzo, P180 promotes the ribosome-independent localization of a subset of mRNA to the endoplasmic reticulum. *PLoS Biol.* **10**, e1001336 (2012).
41. F. Cymer, G. Von Heijne, S. H. White, Mechanisms of integral membrane protein insertion and folding. *J. Mol. Biol.* **427**, 999–1022 (2015).
42. J. P. Ulmschneider, J. C. Smith, S. H. White, M. B. Ulmschneider, In silico partitioning and transmembrane insertion of hydrophobic peptides under equilibrium conditions. *J. Am. Chem. Soc.* **133**, 15487–15495 (2011).
43. P. F. Almeida, A. S. Ladokhin, S. H. White, Hydrogen-bond energetics drive helix formation in membrane interfaces. *Biochim. Biophys. Acta* **1818**, 178–182 (2012).
44. K. R. MacKenzie, Folding and stability of α-helical integral membrane proteins. *Chem. Rev.* **106**, 1931–1977 (2006).
45. M. Javanainen *et al.*, Quantitative comparison against experiments reveals imperfections in force fields' descriptions of POPC–cholesterol interactions. *J. Chem. Theory Comput.* **19**, 6342–6352 (2023).
46. J. R. Wiśniewski, D. Rakus, Multi-enzyme digestion FASP and the 'Total Protein Approach'-based absolute quantification of the Escherichia coli proteome. *J. Proteomics* **109**, 322–331 (2014).
47. P. Viitanen, M. L. Garcia, H. R. Kaback, Purified reconstituted lac carrier protein from *Escherichia coli* is fully functional. *Proc. Natl. Acad. Sci. U.S.A.* **81**, 1629–1633 (1984).
48. H. Vitrac, M. Bogdanov, W. Dowhan, Proper fatty acid composition rather than an ionizable lipid amine is required for full transport function of lactose permease from *Escherichia coli*. *J. Biol. Chem.* **288**, 5873–5885 (2013).
49. N. B. Woodall, Y. Yin, J. U. Bowie, Dual-topology insertion of a dual-topology membrane protein. *Nat. Commun.* **6**, 8099 (2015).
50. N. Fluman, V. Tobiasson, G. Von Heijne, Stable membrane orientations of small dual-topology membrane proteins. *Proc. Natl. Acad. Sci. U.S.A.* **114**, 7987–7992 (2017).
51. M. Seurig, M. Ek, G. Von Heijne, N. Fluman, Dynamic membrane topology in an unassembled membrane protein. *Nat. Chem. Biol.* **15**, 945–948 (2019).
52. H. Yerushalmi, M. Lebendiker, S. Schuldiner, EmrE, an Escherichia coli 12-kDa multidrug transporter, exchanges toxic cations and H+ and is soluble in organic solvents. *J. Biol. Chem.* **270**, 6856–6863 (1995).

Downloaded from https://www.pnas.org by CAS CONSORTIUM CHINESE ACADEMY OF SCIENCES on January 21, 2026 from IP address 159.226.35.236.